Long Rossby Wave Basin-Crossing Time and the Resonance of Low-Frequency Basin Modes

FRANÇOIS PRIMEAU*

Canadian Centre for Climate Modelling and Analysis, Meteorological Service of Canada, University of Victoria, Victoria, British Columbia, Canada

(Manuscript received 12 December 2000, in final form 5 March 2002)

ABSTRACT

The ability of long-wave low-frequency basin modes to be resonantly excited depends on the efficiency with which energy fluxed onto the western boundary can be transmitted back to the eastern boundary. This efficiency is greatly reduced for basins in which the long Rossby wave basin-crossing time is latitude dependent.

In the singular case where the basin-crossing time is independent of latitude, the amplitude of resonantly excited long-wave basin modes grows without bound except for the effects of friction. The speed of long Rossby waves is independent of latitude for quasigeostrophic dynamics, and the rectangular basin geometry often used for theoretical studies of the wind-driven ocean circulation is such a singular case for quasigeostrophic dynamics.

For more realistic basin geometries, where only a fraction of the energy incident on the western boundary can be transmitted back to the eastern boundary, the modes have a finite decay rate that in the limit of weak friction is independent of the choice of frictional parameters. Explicit eigenmode computations for a basin geometry similar to the North Pacific but closed along the equator yield basin modes sufficiently weakly damped that they could be resonantly excited.

1. Introduction

In recent articles, LaCasce (2000) and Cessi and Primeau (2001) have demonstrated that there exists, in the physically relevant case of weak friction, a set of weakly damped low-frequency basin modes. The basin modes consist of a westward propagating long Rossby wave excited by boundary pressure fluctuations at the eastern boundary and a uniform pressure adjustment that enforces mass conservation in the basin. This uniform pressure adjustment is determined by imposing an integral constraint for mass conservation in the basin. Furthermore, it is this pressure adjustment that produces the pressure fluctuations at the eastern boundary. At the western boundary a frictional boundary layer damps out part of the mode's energy so that the resulting modes are weakly damped. The period of the gravest mode is given by the time for long Rossby waves to cross the basin. For midlatitude first baroclinic waves, this time is on the order of a decade. Cessi and Primeau (2001) also show that for the case of a square ocean basin these modes can be resonantly excited by weak atmospheric forcing to produce strong decadal fluctuations in the depth of the thermocline.

For quasigeostrophic (QG) dynamics in a square basin the crossing time, given by the width of the basin divided by the long Rossby wave phase speed, is independent of latitude. Real ocean basins, however, are not square, and their width depends on latitude. Furthermore, real ocean basins have large north–south extent so that the speed of long Rossby waves propagating in them also depends on latitude contrary to the quasigeostrophic approximation. Since the basin-crossing time is actually a function of latitude, it is natural to inquire how the modes identified by Cessi and Primeau (2001) are affected. In a follow-up article, Cessi and Louazel (2001) studied a shallow-water model and found that because of the variations of the long Rossby wave phase speed in the shallow-water model, the decay rate of the basin modes remained finite as the friction parameter was decreased. Here we will investigate the role played by the basin shape in both a quasigeostrophic setting and in a shallow water setting.

To this end, we begin by revisiting in section 2 the quasigeostrophic case previously considered by Cessi and Primeau (2001). The difference is that here we allow the width of the basin to vary with latitude. After having gained an understanding of the quasigeostrophic case with latitude-dependent crossing time, it is straightfor-

* Current affiliation: Department of Earth System Science, University of California, Irvine, Irvine, California.

Corresponding author address: François Primeau, Canadian Centre for Climate Modelling and Analysis, Meteorological Service of Canada, University of Victoria, P. O. Box 1700, Victoria, BC V8W 2Y2, Canada.
E-mail: fprimeau@uci.edu

ward to extend the results to planetary scales via the shallow-water equations in spherical coordinates (section 3). The conclusions are presented in section 4.

2. The quasigeostrophic case

The linear evolution of the transport streamfunction forced by wind stress $\boldsymbol{\tau}$ is governed by

$$\frac{\partial}{\partial t}\left(\nabla^2\psi - \frac{1}{R^2}\psi\right) + \beta\frac{\partial\psi}{\partial x} = \frac{1}{\rho}\,\mathrm{curl}\boldsymbol{\tau} + \kappa\nabla^2\left(\nabla^2\psi - \frac{1}{R^2}\psi\right), \tag{1}$$

where

$$R \equiv \frac{\sqrt{g'H}}{f}, \quad \text{baroclinic deformation radius} \tag{2}$$

and

$$\kappa \equiv \text{large-scale eddy diffusivity.} \tag{3}$$

For geostrophic flow, the kinematic boundary condition of no flow normal to the basin walls requires that there be no pressure gradient along the basin boundary. In a simply connected domain, the resulting boundary condition is that

$$\psi|_{\text{boundary}} = \psi_0(t). \tag{4}$$

The scalar function, $\psi_0(t)$, gives the time evolution of the boundary pressure. It is determined as part of the solution by requiring that the total mass be conserved:

$$\int_{\text{area}} \psi(x, y, t)\, dx\, dy = 0. \tag{5}$$

Because of the fourth-order derivative in the friction term, an additional boundary condition is required, for which one can choose either no-slip or free-slip boundary conditions:

$$\boldsymbol{\nabla}\psi\cdot\mathbf{n} = 0, \quad \text{(no slip)} \tag{6}$$

$$\nabla^2\psi = 0, \quad \text{(free slip).} \tag{7}$$

In order to allow the basin crossing time for long Rossby waves to be a function of latitude within the quasigeostrophic context, we consider a basin whose width is a function of latitude:

$$D = \{(x, y)\,|\,0 \le y \le Y_N,\ X_W(y) \le x \le X_E(y)\}. \tag{8}$$

Here $X_W(y)$ and $X_E(y)$ are the positions of the eastern and western basin boundaries as a function of y, and Y_N is the maximum north–south extent of the basin.

a. Nondimensionalization

It is useful to recast the problem in nondimensional form by introducing the following scales:

$$(x, y) = L_x(x^*, y^*), \tag{9}$$

$$t = t_0 t^*, \tag{10}$$

$$\psi = \tau_0(\beta\rho)^{-1}\psi^*, \tag{11}$$

where time has been nondimensionalized by the time for a long Rossby wave to cross a basin of width L_x,

$$t_0 = \frac{L_x}{\beta R^2}. \tag{12}$$

The resulting nondimensional equation after dropping the asterisks is

$$(\epsilon\nabla^2\psi - \psi)_t + \psi_x = G(x, y, t) + \delta\nabla^2(\epsilon\nabla^2\psi - \psi) \tag{13}$$

in which $G(x, y, t)$ is the wind forcing. The nondimensional boundary conditions are

$$\psi = \psi_0(t), \tag{14}$$

$$\epsilon\delta\boldsymbol{\nabla}\psi\cdot\mathbf{n} = 0, \quad \text{or} \quad \epsilon\delta\nabla^2\psi = 0, \tag{15}$$

together with the integral constraint for mass conservation,

$$\int_D \psi(x, y, t)\, dx\, dy = 0. \tag{16}$$

There are two small parameters

$$\epsilon \equiv \left(\frac{R}{L_x}\right)^2, \qquad \delta \equiv \frac{\kappa}{\beta L_x R^2}. \tag{17}$$

The parameter δ is the ratio of the basin crossing timescale to the damping timescale for long Rossby waves and the parameter ϵ measures the relative importance of inertia to vortex stretching.

For midlatitude scalings,

$$\beta = 2 \times 10^{-11}\ \mathrm{m^{-1}\ s^{-1}}, \tag{18}$$

$$L_x = 8 \times 10^6\ \mathrm{m}, \tag{19}$$

$$R = 3 \times 10^4\ \mathrm{m}, \tag{20}$$

$$\kappa = 1000\ \mathrm{m^2\ s^{-1}}. \tag{21}$$

Typical values for the small parameters are

$$\epsilon = 2.4 \times 10^{-5}, \qquad \delta = 6.9 \times 10^{-3} \tag{22}$$

so that

$$\epsilon \ll \delta \ll 1. \tag{23}$$

b. Numerical method

We will be looking for eigenmode solutions of the form

$$\psi = e^{-i\omega t}\phi(x, y). \tag{24}$$

Substitution into the governing equation yields the following eigen problem:

$$-i\omega[\epsilon\nabla^2\phi - \phi] + \phi_x = \delta\nabla^2(\epsilon\nabla^2\phi - \phi), \quad (25)$$

which can be written as a matrix eigenvalue problem,

$$-i\omega\mathbf{B}\phi = \mathbf{A}\phi, \quad (26)$$

by discretizing the equations. For the solutions presented in the following sections, the discretization approximates the solution using the finite element method on a unstructured mesh made of triangles. The domain triangulation is done using the two-dimensional mesh generator ''Triangle'' available from Netlib (see acknowledgments). The basis functions are first-order tent functions. Second-order tent functions were used as well to check the convergence of the solutions.

c. Long-wave approximation with weak friction

In order to make the long-wave approximation for the solution of modes in a closed basin, it is important that short Rossby waves generated by reflection at the western boundary be damped out sufficiently fast that they will not propagate out of the western boundary layer and spoil the long-wave approximation in the basin interior. Rossby waves reflected from the western boundary must have an eastward group velocity. Consequently, their wavelengths are shorter than the Rossby deformation radius. In terms of our nondimensional parameters, eastward propagating Rossby waves have wavelengths $\lambda \leq \epsilon^{1/2}$ so that their damping time is

$$t_{\text{sw}} \sim O\left(\frac{\psi}{\delta\nabla^2\psi}\right) \leq \frac{\epsilon}{\delta}. \quad (27)$$

Thus for the long-wave approximation to be valid, it is necessary that $\epsilon \ll \delta$ as is the case for scaling (23). The scaling $\epsilon \ll \delta \ll 1$ implies that short Rossby waves with eastward group velocity will be damped quickly by friction, while westward propagating long Rossby waves will be damped slowly with a long timescale, $t_{\text{lw}} \sim O(1/\delta)$.

It is important to distinguish the limit $\epsilon \ll \delta \to 0$ from the alternate limit $\delta \ll \epsilon \to 0$. The former leads to the long-wave basin modes whose properties we focus on in the present paper. The later does not. It leads to the small Rossby radius limit of the inviscid basin modes discussed by Flierl (1977).

Note that if either ϵ or δ vanish, the fourth-order derivatives in the governing equation (13) vanish so that one cannot impose the boundary condition on the tangential velocity. This is why we have multiplied the no-slip or free-slip boundary condition by $\epsilon\delta$ in (15). If both ϵ and δ vanish, then the second-order derivatives in the governing equation also vanish. In this case, the governing equation reduces to a first-order hyperbolic equation, $-\psi_t + \psi_x = G(x, y, t)$ and one can only satisfy the no normal-flow boundary condition (14) at the eastern boundary from which the characteristics emanate. In order to satisfy the no-normal flow boundary condition at the western wall, one must retain either the frictional term or the inertial term depending on which is larger. In contrast, the integral constraint (16) can be satisfied even when both ϵ and δ vanish.

For basin-scale modes, the scaling given by (23) implies that both friction and inertia can be neglected away from thin boundary layers. To $O(\delta)$, the interior problem reduces to

$$\left.\begin{aligned} -\frac{\partial\psi_I}{\partial t} + \frac{\partial\psi_I}{\partial x} &= 0 \\ \psi_I[X_E(y), t] &= \psi_0(t) \end{aligned}\right\}. \quad (28)$$

Again, because of the scaling $\epsilon \ll \delta \ll 1$, the eastward propagating short Rossby waves are damped out before they can leave the frictional western boundary layer. Consequently, the integrand in the integral constraint can be well approximated by the interior long-wave solution ψ_I everywhere except in the frictional boundary layers. Only in the frictional boundary layers are the corrections to ψ_I of order one, but those corrections of order one are confined to a boundary layer of thickness δ so that their contribution in the total integral will only be of order δ:

$$\begin{aligned} \iint \psi \, dx \, dy &= \iint \psi_I + \psi_b \, dx \, dy \\ &= \iint \psi_I + O(\delta). \end{aligned} \quad (29)$$

Thus the interior solution must satisfy the integral constraint

$$\int_0^{Y_N} dy \int_{X_W(y)}^{X_E(y)} dx\{\psi_I\} = 0. \quad (30)$$

1) Energy considerations

The energy equation for the interior problem is obtained by multiplying equation (28) by ψ_I, to get

$$E_t + \nabla\cdot F = 0, \quad (31)$$

in which the energy density is given by $\psi_I^2/2$ and the energy flux is given by

$$\mathbf{F} = -\mathbf{x}\frac{\psi_I^2}{2}. \quad (32)$$

Note that the energy flux is everywhere westward. For a resonant mode to be established, some of the energy fluxed onto the western boundary must be returned to the eastern boundary where it can radiate back into the interior—otherwise the mode will be completely damped out after one long-wave basin-crossing time. As is well known, for inviscid basin modes ($\delta = 0$, $\epsilon \neq 0$), the energy is reflected back to the eastern boundary by short Rossby waves with eastward group velocity. For the long-wave basin modes satisfying scaling

(23) this is not possible since short Rossby waves are damped within a thin western boundary-layer. Cessi and Primeau (2001) demonstrate that in the long-wave limit the time-dependent boundary pressure allows the energy to be transferred back to the eastern boundary. Physically, the boundary pressure adjustment can be thought of as parameterizing the effect of very low-frequency gravity waves forced by the mass redistributions induced by the propagation of long Rossby waves in a closed basin. We will return to this interpretation in section 3 when we consider the shallow-water equations.

Energy considerations allow us to obtain an expression for the energy rate of change in terms of the interior solutions ψ_I, without having to consider the details of the frictional western boundary layer. The incident energy fluxed onto the western boundary layer, F^I, and the energy transmitted to the eastern boundary by the time-dependent boundary pressure, F^T, are given by

$$F^I = \int_0^{Y_N} dy \left[\frac{\psi_I(X_W(y), y, t)^2}{2}\right],$$

$$F^T = \int_0^{Y_N} dy \left[\frac{\psi_0(t)^2}{2}\right]. \tag{33}$$

Note that the interior solution $\psi = \psi_I$ does not satisfy the no-normal flow boundary condition at the western boundary; F^I can be rewritten in a more useful form by making use of the mass conservation constraint. Differentiating (30) with respect to time and using (28) gives

$$\int_0^{Y_N} dy\{\psi_I(X_W(y), y, t)\} = \int_0^{Y_N} \psi_0(t)\, dy,$$

whence, the boundary pressure term is given by the meridional average of the interior solution evaluated along the western boundary

$$\psi_0(t) = \frac{1}{Y_N}\int_0^{Y_N} \psi_I(X_W(y), y, t)\, dy. \tag{34}$$

If we then decompose $\psi_I(X_W(y), y, t)$ into an average plus deviation,

$$\psi_I(X_W(y), y, t) = \psi_0(t) + \psi_I'(y, t), \tag{35}$$

where $\psi_I'(y, t) \equiv \psi(X_W(y), y, t) - \psi_0(t)$, the incident energy fluxed onto the western boundary can be written as

$$F^I = \frac{1}{2}\int_0^{Y_N} (\psi_0^2 + (\psi_I')^2)\, dy$$

since $\int_0^{Y_N} \psi'\, dy = 0$. Note that if the basin-crossing time is independent of latitude, the wave fronts arrive at the western boundary with their lines of constant phase parallel to the wall. In that case $\psi_I(X_W(y)) = \text{const}$ and $\psi' = 0$.

Since there is no dissipation in the interior of the basin, the difference between the energy incident on the western boundary and the energy transmitted to the eastern boundary gives the rate of change of total energy,

$$\begin{aligned}\int_D E_t &= -(F^I - F^T)\\ &= -\int_0^{Y_N} dy\left(\frac{\psi_0^2}{2} + \frac{(\psi_I')^2}{2}\right) + \int_0^{Y_N} dy\frac{\psi_0^2}{2}\\ &= -\int_0^{Y_N} \frac{(\psi_I')^2}{2} \le 0.\end{aligned}$$

Thus we see that the total energy must decrease unless $\psi_I' = 0$, that is, unless the wave fronts arrive at the western boundary parallel to the wall. This will be the case only if the basin-crossing time for long waves is independent of latitude.

The reflection process at the western boundary splits the energy into two parts. One part is reflected into the uniform boundary pressure adjustment. The other part that is reflected into the short eastward propagating Rossby waves is quickly damped out in the frictional boundary layer. The energy partitioning is determined by the meridionally averaged long-wave interior solution evaluated along the western boundary. The part of the energy that is reflected into the uniform pressure adjustment is transmitted to the eastern boundary where it excites the long Rossby waves.

The square basin considered by Cessi and Primeau (2001) is a singular case since the basin crossing time for long Rossby waves is independent of latitude. This is why the amplitude of the resonating basin modes becomes unbounded as the friction parameter δ approaches zero. In general, however, the long-wave basin-crossing time will not be independent of latitude and the resonating basin modes will have a finite amplitude even as the friction parameter approaches zero.

2) FREE MODES

Cessi and Louazel (2001) show that it is possible to obtain an estimate of the period and damping time of free modes of the planetary geostrophic equations without having to deal explicitly with the frictional boundary layers. If we apply their method to the quasigeostrophic equations we can make the connection to the inviscid results of Cessi and Primeau (2001) more direct. For this method, we consider free mode solutions of the form $\psi(x, y, t) = e^{\sigma t}h(x, y)$. Substitution into (28) and a little algebra yields

$$\psi = h_0 e^{\sigma(x - X_E(y) + t)}, \tag{36}$$

where σ is yet to be determined and h_0 is an arbitrary amplitude independent of x and y. The conservation of mass constraint (16) yields an equation for σ,

$$\int_0^{Y_N} dy\left\{\frac{1}{\sigma}(1 - e^{\sigma(X_W(y) - X_E(y))})\right\} = 0. \tag{37}$$

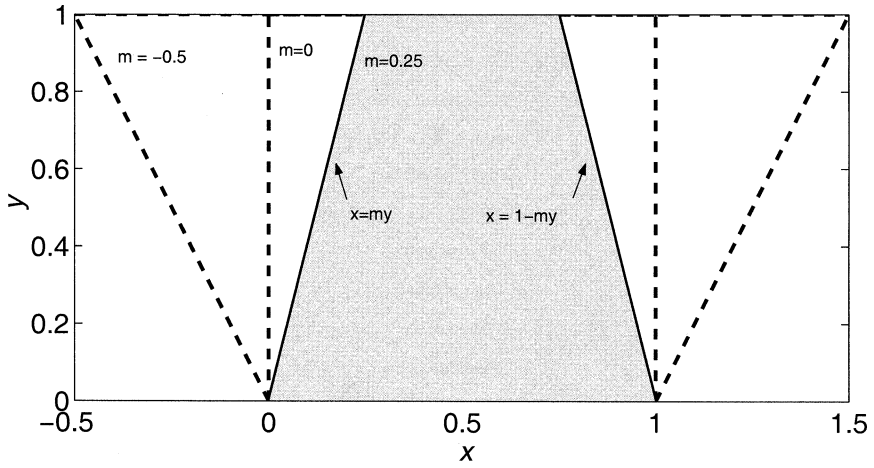

FIG. 1. Basin geometry for various values of the parameter m. For $m = 0$ the basin geometry is square, for $m < 0$ it wider to the north, and for $m > 0$ it is narrower to the north.

For the special case where the width of the basin is independent of y; for example, $X_E(y) - X_W(y) = 1$, Eq. (37) reduces to

$$1 - e^{\sigma} = 0, \tag{38}$$

and we recover the purely oscillatory undamped solutions found by Cessi and Primeau (2001),

$$\sigma = i2\pi n \quad \text{for} \quad n = 1, 2, \cdots. \tag{39}$$

Basins with latitude independent widths allow the long-wave basin modes to resonate most strongly. To study the effect of basins with varying width, we consider the special case of straight, but nonparallel, western and eastern boundaries with $Y_N = 1$:

$$X_w(y) = my, \qquad X_E(y) = 1 - my, \qquad m < 1/2. \tag{40}$$

Figure 1 shows the basin domain. For $m = 0$ we have a square basin. For $m > 0$ we have a basin that narrows to the north, and for $m < 0$ we have a basin that is wider in the north. Note that the maximum crossing-time for long waves as a function of latitude is given by

$$t_{\max} = \begin{cases} 1 - 2m, & m < 0 \\ 1, & m \geq 0. \end{cases} \tag{41}$$

For the choice of basin geometry (40), the y integration in (37) can be carried out explicitly, and the integral constraint reduces to an algebraic equation for σ,

$$\frac{1}{\sigma}\left\{1 - \frac{1}{2m\sigma}(e^{\sigma(2m-1)} - e^{-\sigma})\right\} = 0. \tag{42}$$

For $m \neq 0$, solutions for σ are obtained numerically. Figures 2 and 3 show the frequency, Im$\{\sigma\}$, and e-

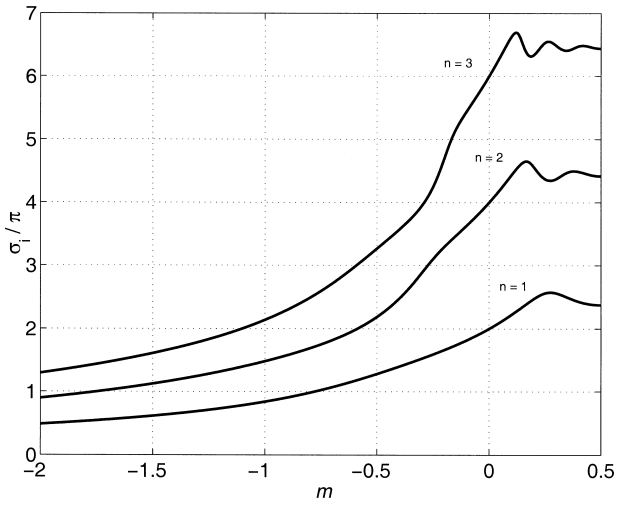

FIG. 2. Frequency of the gravest mode as a function of m. For $m = 0$, the basin width is independent of y.

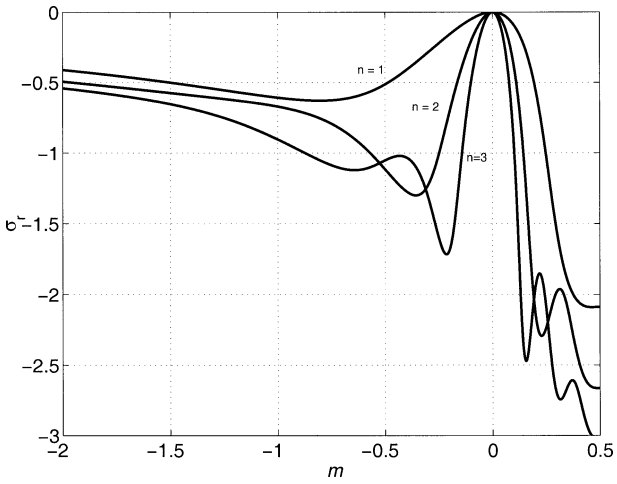

FIG. 3. Damping rate of the gravest mode as a function of m. For $m = 0$, the basin width is independent of y.

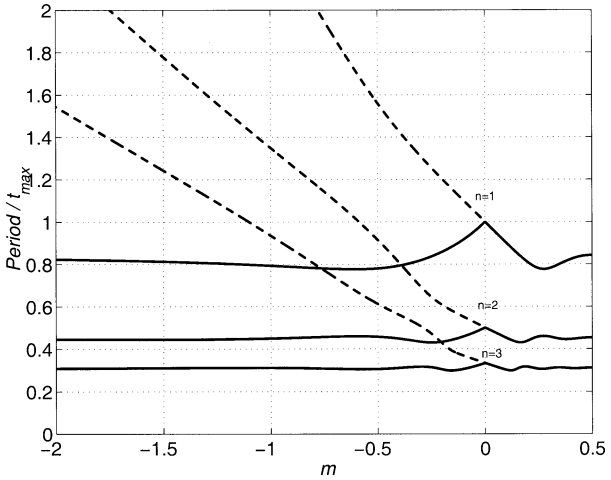

FIG. 4. Period of the three modes (dashed lines) as a function of *m*, as well as the period of the three modes rescaled by the maximum basin-crossing time t_{max} (solid curves) as a function of *m*.

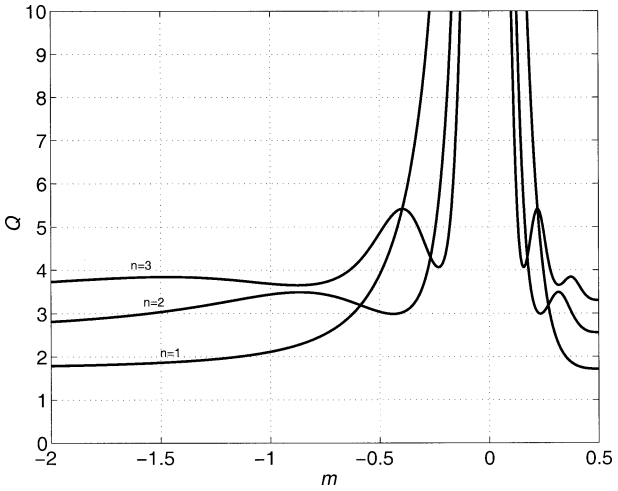

FIG. 5. Plot of *Q* factors for the three modes as a function of *m*. As $m \to 0$, the basin width becomes independent of latitude, and $Q \to \infty$.

folding decay rate, $\mathrm{Re}\{\sigma\}$, for the three gravest modes. We first discuss the frequency of the modes as a function of the basin geometry. For $m > 0$, the basin narrows to the north and the maximum basin-crossing time for long waves is independent of *m*, the frequency remains relatively constant. For $m < 0$, where the basin widens to the north, however, the frequency decreases with *m*. In Fig. 4, a plot of the period of the three gravest modes, rescaled by the maximum crossing time, shows that the rescaled period varies little as *m* is varied in comparison to the non-rescaled period. This indicates that the period of the modes scales as the maximum basin-crossing time for long Rossby waves.

If we now consider the damping of the modes (Fig. 3), we find that even though friction was neglected in obtaining the approximate long-wave solutions, the modes have a finite damping rate except for the special case $m = 0$ (the square basin case). Thus, as long as the friction is sufficiently small, the damping rate of long-wave modes is to first-order independent of friction. The amplitude of the resonantly excited long-wave basin modes does not depend on the explicit value of the dissipation parameter. Instead, it is determined by the shape of the basin. This is a satisfying result since frictional parameters—apart from being small—are poorly known.

For the special case of $m = 0$, the damping rate goes to zero in the absence of explicit friction. This is due to the fact that when the long Rossby wave basin-crossing time is independent of latitude, the energy carried westward by the long Rossby-wave component of the mode is perfectly reflected into the parameterized forced gravity wave component of the mode. There is not in this case a fixed fraction of the energy that is trapped near the western boundary where it can be efficiently damped out by friction. In these special basins the amplitude of resonantly excited long-wave basin modes depends on the explicit value of the friction parameter.

3) RESONANCES

Cessi and Primeau (2001) showed that the long-wave low-frequency basin modes can be resonantly excited. Given that the square basin geometry they considered is optimally suited to produce resonances, one must ask if resonances are possible in more general basin geometries. The ability of resonators to produce spectral peaks can be measured in terms of the ''quality factor'' or *Q*-factor (e.g., Marion 1970). For our modal solutions, the *Q* factor is

$$Q \equiv \omega_r/(2\sigma_r), \tag{43}$$

where $\omega_r = (\sigma_i^2 - \sigma_r^2)^{1/2}$ is the frequency at which the resonantly excited mode would produce a spectral peak. Real positive *Q* factors give spectral peaks, with the sharpness of the spectral peak increasing with increasing *Q* factors. Usually, only broad spectral peaks are present in geophysical records. For reference, Wunsch (2000) points out that the prominent El Niño–Southern Oscillation index signal has a $Q \sim 1$. Thus, if long-wave modes have real *Q* factors, they have the potential of being resonantly excited by stochastic atmospheric forcing. In the real ocean, their ability to resonate would of course be reduced by frictional dissipation and mode coupling, which would drain energy out of the modes.

In Fig. 5, the *Q* factors for the three gravest modes are plotted as a function of *m* for the basin geometry considered in Fig. 1. For $m = 0$, the *Q* factors go to infinity because of the absence of explicit friction, pointing to the fact that the square basin is an ideal resonating cavity for long-wave basin modes. For $m \neq 0$ the *Q* factors are greater than unity, indicating that long-wave

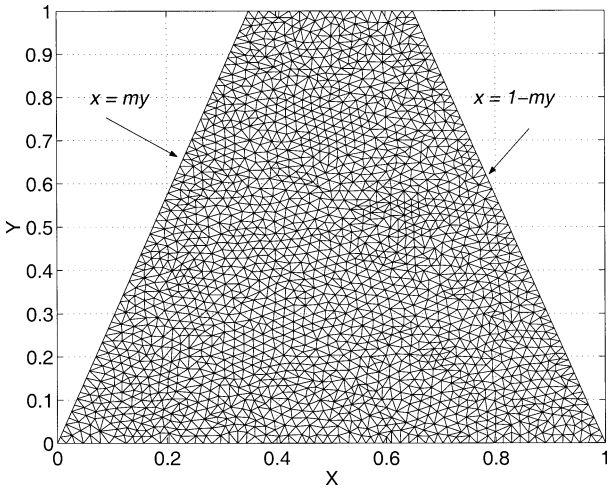

FIG. 6. Basin domain showing a typical unstructured triangular mesh.

basin modes can be resonantly excited even when the basin-crossing time is latitude dependent.

d. Basin mode computations with inertial and frictional effects

To confirm the results obtained in the previous section, we carry out explicit two-dimensional eigenmode computations retaining inertial effects ($\epsilon \neq 0$) and with friction in the form of Rayleigh drag. With Rayleigh drag, only the no normal-flow boundary condition is imposed along the basin boundary. We use a finite element method with linear elements for an unstructured triangular mesh, as well as quadratic elements to check for convergence. Figure 6 shows a typical mesh.

For the two-dimensional computations, we choose $\epsilon = 0.001\,25$ and vary δ and m, and seek modal solutions of the form $\psi = e^{\sigma}h(x, y)$. Typical eigenmodes are shown in Fig. 7 where the two gravest modes are contoured for a basin which is wider to the north ($m = -0.5$, $\delta = 0.01$). Lines of constant phase arrive at the western boundary at an angle. Friction in the thin western boundary layer forces the phase to become constant along the wall such that the no normal-flow boundary condition can be satisfied. Note how the lines of constant phase are parallel to the eastern boundary as they propagate westward. In contrast, inviscid basin modes for which inertial effects allow the no-normal flow boundary conditions to be satisfied have their phase lines perpendicular to lines of constant planetary vorticity (Flierl 1977), regardless of the basin shape. With $\epsilon \leq \delta$, short Rossby waves with eastward group velocity cannot propagate far from the western wall before being damped out. Thus only westward propagating long waves are present in the eastern part of the basin. Note also that, at any given time, the amplitude of the mode increases westward. This can be understood mathematically because the dynamical balance for the long-wave

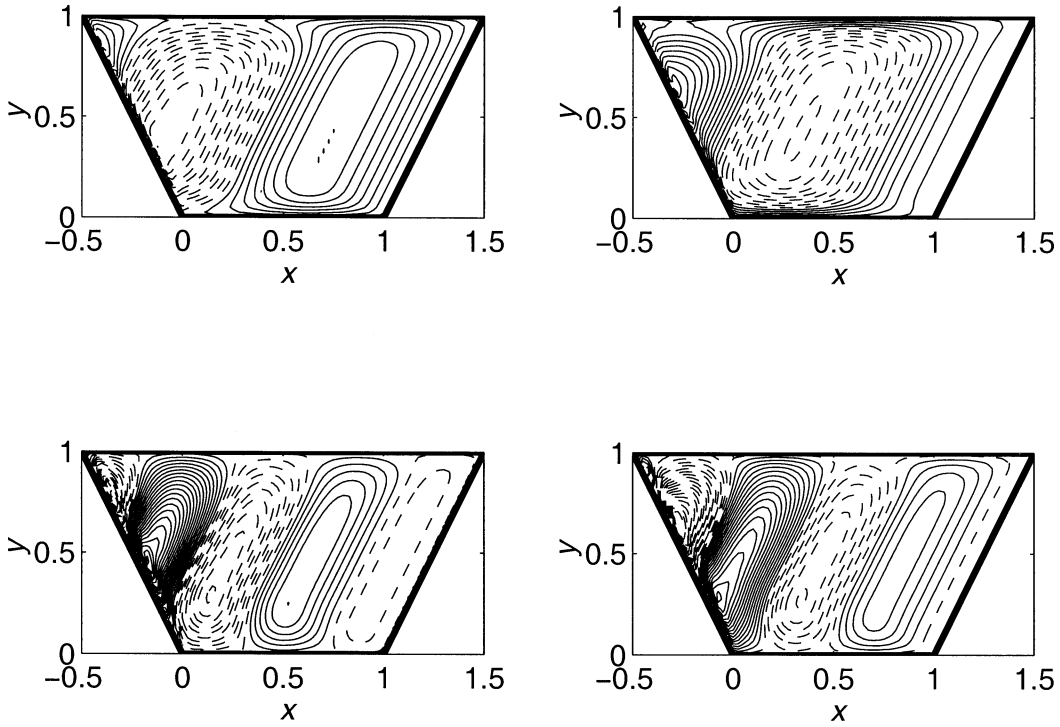

FIG. 7. Real and imaginary parts for the gravest mode (top two panels), and of the second gravest mode (bottom two panels), for $m = -0.5$ and $\delta = 0.05$. Solid contours indicate positive values, and dashed contours indicate negative values.

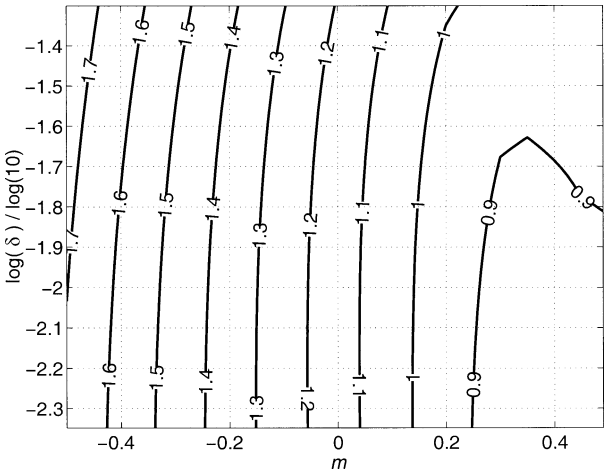

FIG. 8. Period of the gravest basin mode as a function of the logarithm of the frictional parameter $\log_{10}\delta$, and the geometry parameter m. The period is nondimensionalized by the basin-crossing time for long waves in a square basin.

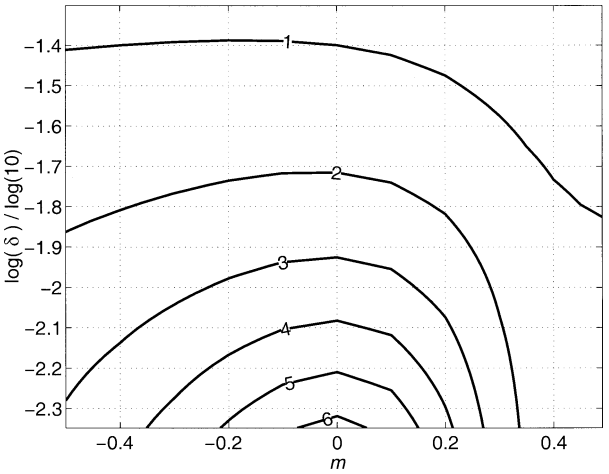

FIG. 9. Plot of Q factors for the gravest basin mode as a function of the log of the frictional parameter $\log_{10}\delta$ and the geometry parameter m. Parallel eastern and western walls have $m = 0$.

basin modes is governed by a first-order hyperbolic equation, whose solution must be of the form $f(x + t)$. Modal solutions must therefore be of the form $A(y)e^{\sigma(x+t)}$. From this functional form we can see that the mode's amplitude must decay in the eastward direction if it is decaying in time. Physically, this can be understood by the fact that the decaying mode produces a decaying pressure oscillation at the eastern boundary. The boundary pressure fluctuations are then carried westward by the long Rossby waves. Since dissipation in the basin interior is negligible, the fluctuations in the western part of the basin having originated at a much earlier time than those nearer to the eastern boundary have a larger amplitude.

In Fig. 8 the period of the gravest mode is contoured as a function of the frictional parameter δ and the parameter m controlling the basin geometry. For a narrowing basin with $m > 0$, the period of the modes is close to unity (recall that time is nondimensionalized by the basin-crossing time for long waves in the southern part of the basin). For a widening basin with $m < 0$, the period increases along with the increase in the maximum width of the basin, in agreement with the long-wave results of the previous section.

Figure 9 contours the Q factor for the gravest mode as a function of the basin geometry m and the friction parameter δ. The best resonators occur for $m = 0$. The ability of the modes to be resonantly excited decreases as m moves away from zero. As the friction parameter δ is decreased there is a rapid increase in the Q factor for the case $m = 0$ in accordance with the long-wave results presented in the previous section. Note that there is a wide range of frictional parameters with $Q \sim O(1)$ even with finite friction in basins for which the lines of constant phase arrive at the western boundary at a large angle. Thus, the conclusion of Cessi and Primeau (2001) that long-wave basin modes can be resonantly excited remains valid for more general basin geometry. The difference is that, for weak friction, the damping of the modes in basins with latitude dependent width is not controlled by the choice of dissipation parameterization as is the case for the special choice of a square ocean basin.

3. Planetary geostrophic case

In this section we demonstrate how the understanding gained from the quasigeostrophic case carries over to the shallow-water equations. The structure of the long-wave modes is essentially unchanged; one simply has to take into account the variations of the phase speed with latitude in addition to the variations of the basin width when determining the variations of the basin-crossing time with latitude. Furthermore, the shallow-water equations retain the necessary dynamics for mass conservation. Consequently, the long-wave basin modes computed using the shallow-water equations will explicitly resolve the dynamical process that transmits the energy back to the eastern boundary.

The linearized shallow water equations, with friction in the form of Rayleigh drag, can be written in spherical geometry as follows:

$$u_t - fv = -g'h_\lambda/(a\cos\phi) - ru, \tag{44}$$

$$v_t + fu = -g'h_\phi/a - rv, \tag{45}$$

$$h_t + H\nabla_h \cdot \mathbf{u} = 0. \tag{46}$$

The first two equations are the momentum equations, and the third is the conservation of mass equation, with $f = 2\Omega\sin\phi$ the Coriolis parameter, a the radius of the earth, r the Rayleigh friction parameter, g' the reduced gravity, and h the displacement of the layer depth about the mean depth H. Unlike the QG formulation, the shal-

low-water equations retain gravity wave motions and conserve mass without the need to impose the integral constraint for mass conservation.

For modes with a decadal period, $\omega \sim 2 \times 10^{-8}\ \mathrm{s}^{-1}$, the tendency terms in the momentum equations are small compared with the Coriolis, pressure gradient, and friction terms. We can therefore neglect the tendency terms in the momentum equations. The neglect of these terms filters out the free gravity modes from the problem as well as the short Rossby waves:

$$-fv = -g'h_\lambda/(a\cos\phi) - ru, \tag{47}$$

$$+fu = -g'h_\phi/a - rv. \tag{48}$$

$$h_e + H\nabla_h\cdot\mathbf{u} \tag{49}$$

This approximation while correct for realistic parameter values will break down in the limit of zero friction. Eliminating u and v from (49) to obtain a single equation in h and letting $r \to 0$ gives

$$\frac{\partial h}{\partial t} - \frac{c(\phi)}{a\cos\phi}\frac{\partial h}{\partial \lambda} = 0, \tag{50}$$

where

$$c(\phi) = \beta\frac{g'H}{f^2}, \qquad \beta = \frac{2\Omega\cos\phi}{a}. \tag{51}$$

For the basin geometry given by

$$D = \{(\phi, \lambda)\,|\,\Phi_S < \phi < \Phi_N,\ \Lambda_W(\phi) \le \lambda \le \Lambda_E(\phi)\},$$

the long-wave basin-crossing time is given by

$$t_0(\phi) = \frac{(\Lambda_E(\phi) - \Lambda_W(\phi))a\cos\phi}{c(\phi)}. \tag{53}$$

To emphasize the importance of the latitude dependence of the basin-crossing time over the latitude dependence of the phase speed or the basin width we consider two cases. For the first we consider an idealized basin geometry in which the basin width decreases to the north in such a way that the basin-crossing time is independent of latitude. Specifically, we choose the following basin geometry:

$$D = \left\{(\lambda, \phi)\,\middle|\, \frac{-c(\phi)T_0}{2a\cos\phi} \le \lambda \le \frac{c(\phi)T_0}{2a\cos\phi},\right.$$
$$\left.\frac{25\pi}{180} \le \phi \le \frac{80\pi}{180}\right\}, \tag{54}$$

where $T_0 = 15$ yr. For this case we will show that the decay rate of the modes is determined by the friction in an analogous fashion to the case of a rectangular basin for quasigeostrophic dynamics. In contrast, the second case we consider uses the realistic North Pacific basin coastline with a wall along the equator. We chose to close the North Pacific basin in order to avoid having to compute the modes for the entire globe. For this latter case, the basin-crossing time is latitude dependent. Because of this, the wave fronts do not arrive at the western boundary parallel to the basin wall and part of the energy carried by the long Rossby waves becomes trapped near the boundary where it is damped out by friction, giving the modes a finite decay rate even as friction goes to zero.

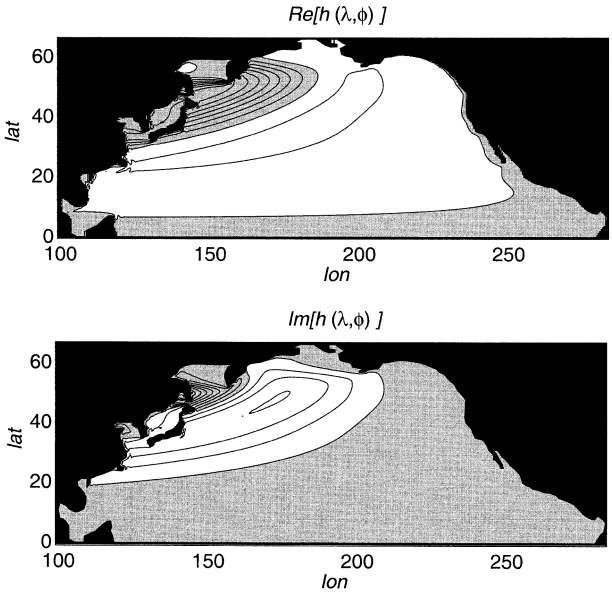

FIG. 10. Real (top panel) and imaginary (bottom panel) parts of the gravest eigenmode for the Pacific basin with a wall along the equator. Shaded areas indicate negative contours ($r = 3 \times 10^{-7}\ \mathrm{s}^{-1}$).

In the following computations we vary the friction parameter r and hold the reduced gravity g' and H fixed ($g' = 0.013\ \mathrm{m\ s}^{-2}$, $H = 1000$ m). Varying $g'H$ changes the period and the decay rate of the modes, but does not change the Q factors. Contour plots of the two gravest modes for the Pacific basin coastline with a wall along the equator are given in Figs. 10 and 11 ($r = 3 \times 10^{-7}\ \mathrm{s}^{-1}$). For our choice of $g'H$, the period of the two gravest modes are 14.2 and 7.0 yr. The gravest mode for the optimally resonating basin is given in Fig. 12 ($r = 3 \times 10^{-7}\ \mathrm{s}^{-1}$). For our choice of $g'H$ its period is 17.2 yr. For the North Pacific basin the phase lines do not arrive parallel to the western boundary. Consequently, a considerable fraction of the energy fluxed onto the western boundary will not be transmitted to the eastern boundary. In contrast, for the optimal basin geometry the phase lines arrive at the western boundary parallel to the wall. Except for the effects of the explicit frictional dissipation, all of the energy incident on the western boundary in the basin with optimal shape is transmitted to the eastern boundary. Figure 13 shows a plot of the Q factors for the two gravest modes in the two different basin geometries. The Q factors for the modes in the optimal-resonator basin shape tend to infinity as the friction tends to zero. In contrast, for the North Pacific geometry, the Q factors tend to a finite limit as the friction goes to zero ($Q \approx 0.6$ for the gravest

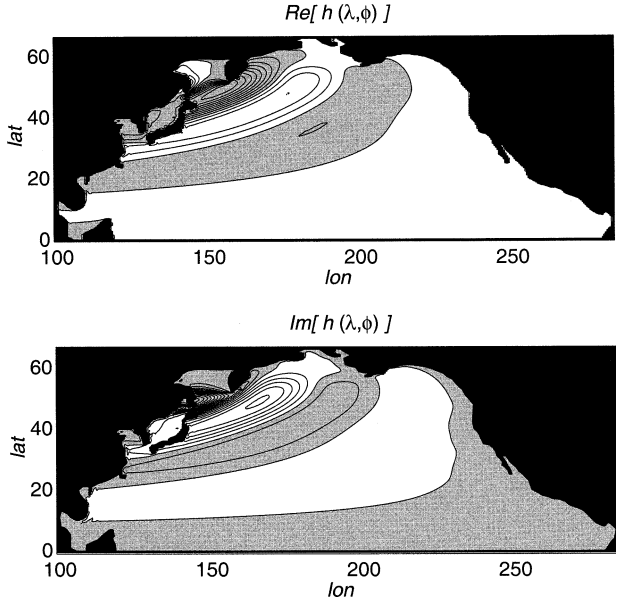

FIG. 11. As in Fig. 10 but for the second gravest eigenmode.

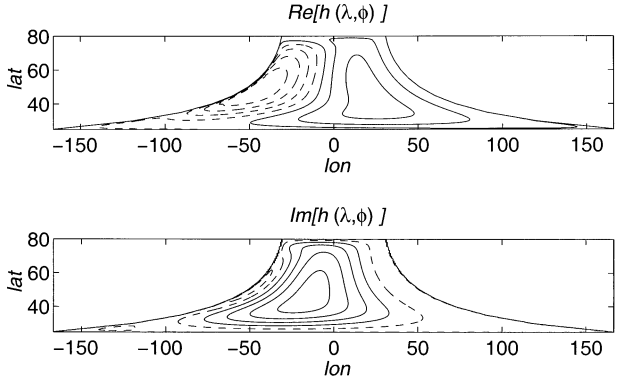

FIG. 12. Real (top panel) and imaginary (bottom panel) parts of the gravest eigenmode for an optimally resonating basin on the sphere. Dashed contours indicate negative values ($r = 3 \times 10^{-7}\ \mathrm{s}^{-1}$).

mode and $Q \approx 1.2$ for the second gravest mode). Nevertheless, the computation for the North Pacific basin shows that even for very irregular basin geometries the long-wave basin modes have Q factors of order one. This suggests that these basin modes might be detectable in the real ocean if they are being excited. Of course the present calculations are restricted to a basin closed off at the equator—a more accurate calculation would solve the problem for the basin configuration of the entire globe. We have neglected nonlinear effects that might become large in the western boundary layer. Also neglected is the effect of the mean background current. For the linearized reduced-gravity formulation mean currents have no effect on the modes because there is an exact cancellation between the Doppler shift and the potential vorticity gradient caused by the thickness gra-

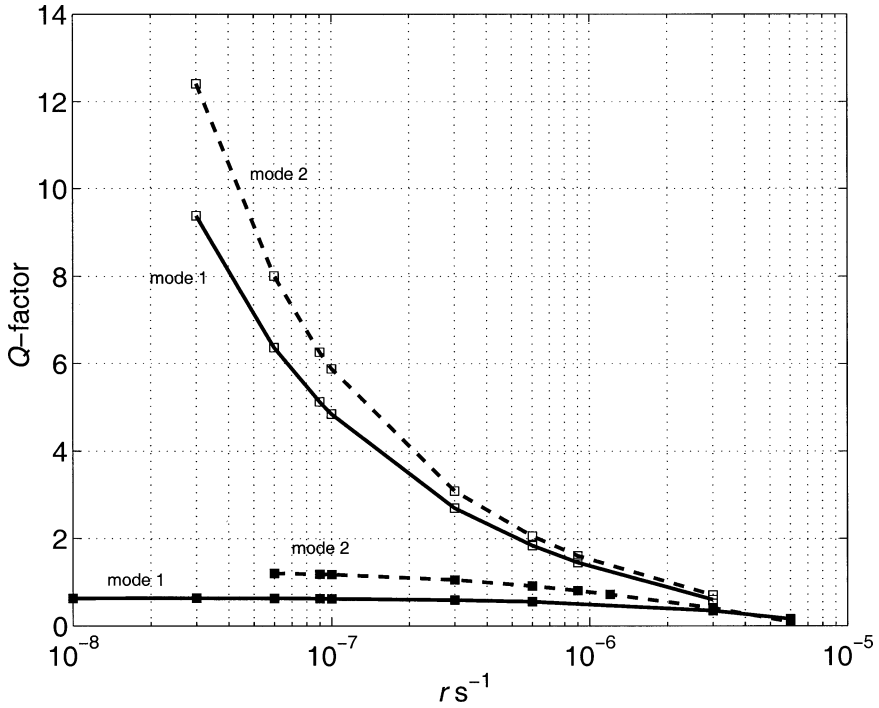

FIG. 13. Plot of the Q factor for the two gravest modes for two different basin geometries as a function of the frictional parameter r. The solid squares are for the North Pacific basin geometry and the open squares are for the optimally resonating basin geometry. The solid lines are for the gravest mode and the dashed line are for the second gravest mode.

dients supporting the flow. For more realistic model formulations with several vertical modes this would no longer be the case. Topography would also act to scatter energy between different vertical modes. It would be interesting to investigate such effects in a future study.

4. Shallow water case

In the previous section's calculations using the planetary geostrophic equations, we neglected the tendency terms in the momentum equations. This approximation is appropriate for low-frequency modes but it also has the effect of filtering out the free gravity waves in general, and Kelvin waves in particular. In the QG formulation, the uniform boundary pressure fluctuations are sometimes said to parameterize the effects of Kelvin waves propagating around the boundary. The uniformity of the pressure adjustment along the boundary is loosely attributed to the fact that for the QG formulations the gravity waves propagate around the boundary instantaneously. Our goal here is to retain the tendency terms in the shallow-water equations so that we can investigate what role, if any, is played by Kelvin waves in the boundary pressure adjustment of the long Rossby wave basin modes.

To address this question we have performed an additional set of computations with the linearized shallow-water equations in which we retain the time derivative terms in the momentum equations. For simplicity, we formulate the problem in Cartesian coordinates on a β plane in a rectangular basin of dimension $L_x = 6000$ km and $L_y = 4000$ km:

$$u_t - (f_o + \beta y)v = -g'h_x - ru, \tag{55}$$

$$v_t + (f_o + \beta y)u = -g'h_y - rv, \tag{56}$$

$$h_t + H(u_x + v_y) = 0. \tag{57}$$

We choose the following numerical values for the parameters $H = 1000$ m, $f_o = 9 \times 10^{-5}$ s^{-1}, $\beta = 1.8 \times 10^{-11}$ m^{-1} s^{-1}, $g' = 0.081$ m s^{-2}, and $r = 1 \times 10^{-6}$ s^{-1}. With these parameters, free gravity waves propagate with a speed of 9 m s^{-1}, and the Rossby radius of deformation ranges from 166 km in the south of the basin to 71 km in the north of the basin. This is larger than for the real ocean, but allows for adequate resolution of motions on the scale of the Rossby radius of deformation without an exceedingly fine grid interval.

Using a finite difference approximation with a 20-km resolution, we first seek free mode solutions in the form

$$\begin{bmatrix} u(x, y, t) \\ v(x, y, t) \\ h(x, y, t) \end{bmatrix} = \begin{bmatrix} \hat{u}(x, y) \\ \hat{v}(x, y) \\ \hat{h}(x, y) \end{bmatrix} e^{i\omega t}. \tag{58}$$

In Fig. 14 we contrast two very different basin modes obtained using the above model formulation. The mode in the upper panel has a period of only 25 days and consists of one counterclockwise propagating gravity wave trapped within one Rossby radius of the coast. Its period is roughly given by the time for a Kelvin wave to propagate around the boundary

$$(2L_x + 2L_y)/\sqrt{g'H} \approx 26 \text{ days}.$$

It corresponds to the gravest mode obtained by Rao (1966) for an inviscid f-plane formulation. In contrast, the mode in the lower panel has a period of 566 days. It is the gravest long Rossby wave basin mode. Its period is comparable to the basin-crossing time for the long

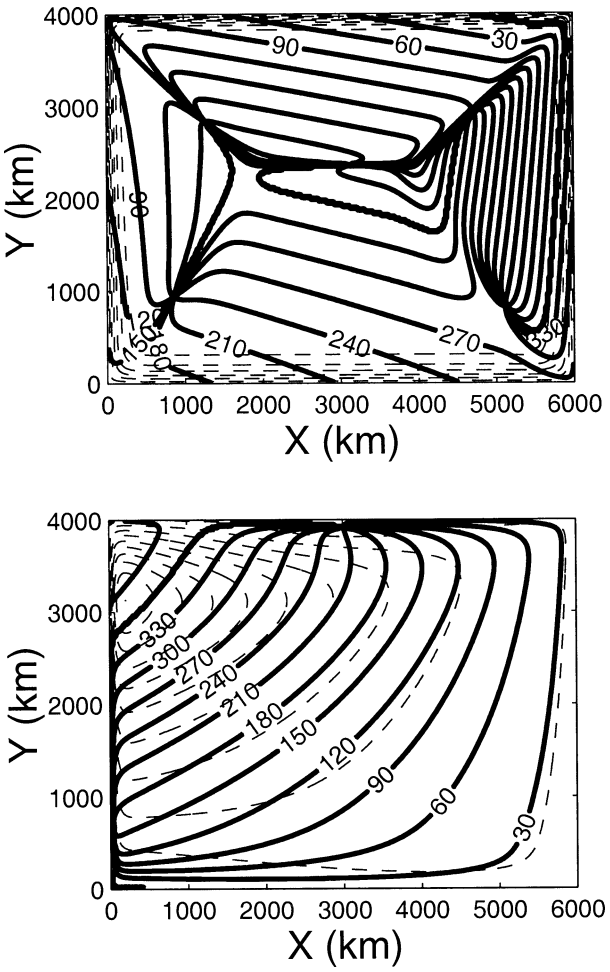

FIG. 14. Gravest ''Kelvin'' mode (upper panel) and gravest long-wave Rossby mode (lower panel). The thick solid and dashed lines denote the phase (cotidal lines) and the amplitude (co-amplitude lines). The contour interval for the amplitude lines is 0.1. (upper panel) The amplitude is unity along the boundary and decreases to zero toward the interior. (lower panel) The amplitude is zero at the amphidromic point ($X \approx 3000$ km, $Y \approx 3900$ km) and increases to unity near the western boundary at ($X \approx 200$ km, $Y \approx 3000$ km). The mode in the upper panel consists of one wave traveling counterclockwise with its amplitude trapped near the boundary and decaying toward the center of the basin with an *e*-folding scale equal to the local Rossby deformation radius. Note how there is a clear phase propagation along the boundary for the ''Kelvin'' mode, but that the phase for the long-wave Rossby mode is nearly constant along the boundary. For the Rossby mode, the boundary pressure oscillates in time but is nearly spatially uniform.

Rossby wave in the north of the basin ($L_x/(\beta R d^2) \approx$ 756 days).

For the ''Kelvin'' mode in the upper panel, the phase propagates around the boundary of the basin in the counterclockwise direction. The pressure along the boundary is clearly a function of *both* space and time. For the long Rossby wave basin mode, the phase propagates westward in the interior of the basin but is nearly constant along the boundary. Unlike the ''Kelvin'' mode the boundary pressure for the long Rossby wave mode is nearly independent of space. It oscillates in time synchronously at all points along boundary despite the fact that the model formulation has a finite Kelvin wave propagation speed. This is not surprising since the time for a gravity wave to propagate around the boundary (26 days) is much shorter than the period of the mode (566 days). This suggests that free Kelvin waves are not the means by which the energy fluxed onto the western boundary by the long Rossby wave is returned to the eastern boundary.

To further examine how the energy is transmitted from the western boundary to the eastern boundary, we now turn to a forced problem in which we prescribe the pressure along the western boundary to oscillate in time. This forcing provides a source of energy at the western boundary. For low-frequency oscillations it is meant to mimic the pressure perturbations caused by the long Rossby waves incident on the western boundary. The boundary forcing is imposed by prescribing thickness along the western boundary as follows:

$$h(x = 0, y, t) = e^{i\omega t}. \tag{59}$$

The response to the prescribed forcing is obtained on an f plane as well as on a β plane. The advantage of the f-plane formulation is that by setting β to zero we can eliminate the Rossby waves and thus isolate the mechanism by which the boundary pressure fluctuations on the western boundary are transmitted to the eastern boundary.

The solution to two different forcing frequencies are contrasted in Fig. 15. The two upper panels show the forced response with $\omega = 2\pi/756$ days, and the lower panels show the forced response with $\omega = 2\pi/25$ days. The left panels are for the f-plane case and the right panels are for the β-plane case. For the high-frequency forcing (lower panels) the response is very similar for both the f-plane and β-plane solutions. There is a clear counterclockwise phase propagation, and the amplitude is trapped near the boundary with an e-folding decay scale equal to the Rossby radius of deformation. For the low-frequency forcing (upper panels), the case with the β-effect (top right panel) shows long Rossby waves radiating from the eastern boundary, indicating that the forcing imposed on the western boundary has been transmitted to the eastern boundary. It is important to note that the response to the low-frequency forcing does not have any phase propagation along the boundary. The pressure around the boundary oscillates synchronously for both the β-plane case and the f-plane case. Furthermore, the low-frequency forced response on the f-plane does not have the typical characteristics associated with free Kelvin wave. There is no phase propagation with the coast to the right, and the amplitude of the response decays away from the boundary with an e-folding scale, that is much larger than one Rossby radius of deformation as is the case for Kelvin waves. (Compare the dashed co-amplitude lines in the upper left panel with those in the lower left panel. The contour interval is the same in both panels).

For the low-frequency long Rossby wave basin modes the boundary pressure fluctuations are spatially uniform even when the speed of the gravity waves is finite. Thus, for motions with frequencies that are much lower than the time for a Kelvin wave to propagate around the perimeter of the basin the uniform boundary pressure adjustment in the QG formulation can not be interpreted as being the manifestation of Kelvin waves propagating around the boundary instantaneously. The mechanism by which the energy of the long Rossby wave modes is transmitted from the western boundary to the eastern boundary is attributed to a low-frequency forced gravity wave response.

The midlatitude long-wave basin modes are different in this respect from the equatorial basin modes described by Cane and Sarachik (1977) and Cane and Moore (1981). For the equatorial modes, the energy carried westward by the Rossby waves is returned eastward by a propagating Kelvin wave. For the midlatitude long-wave Rossby basin modes the resulting modal frequency is so low that the long Rossby waves do not excite any free gravity waves. Instead, they produce a forced gravity wave response at the modal frequency. This forced large-scale response enforces mass conservation and carries energy back to the eastern boundary where it can radiate again as long Rossby waves.

5. Conclusions

If long-wave basin modes are to have a damping timescale longer than the basin-crossing time so as to avoid being damped away, it is necessary for the energy carried westward by the long Rossby waves to be returned to the eastern boundary. In the inviscid theory of Rossby basin modes, this is achieved by the reflection of short Rossby waves at the western boundary. For low frequencies, the resulting inviscid basin modes have small spatial scales, and we would expect that they would be quickly damped out by frictional effects. However, as Cessi and Primeau (2001) have demonstrated, the time-dependent boundary pressure adjustment necessary to conserve mass in the quasigeostrophic limit allows the energy incident on the western boundary to be transmitted back to the eastern boundary without being damped out. In the quasigeostrophic case, the energy is returned to the eastern boundary by the spatially uniform boundary pressure fluctuations. In the shallow-water equations a similar spatially

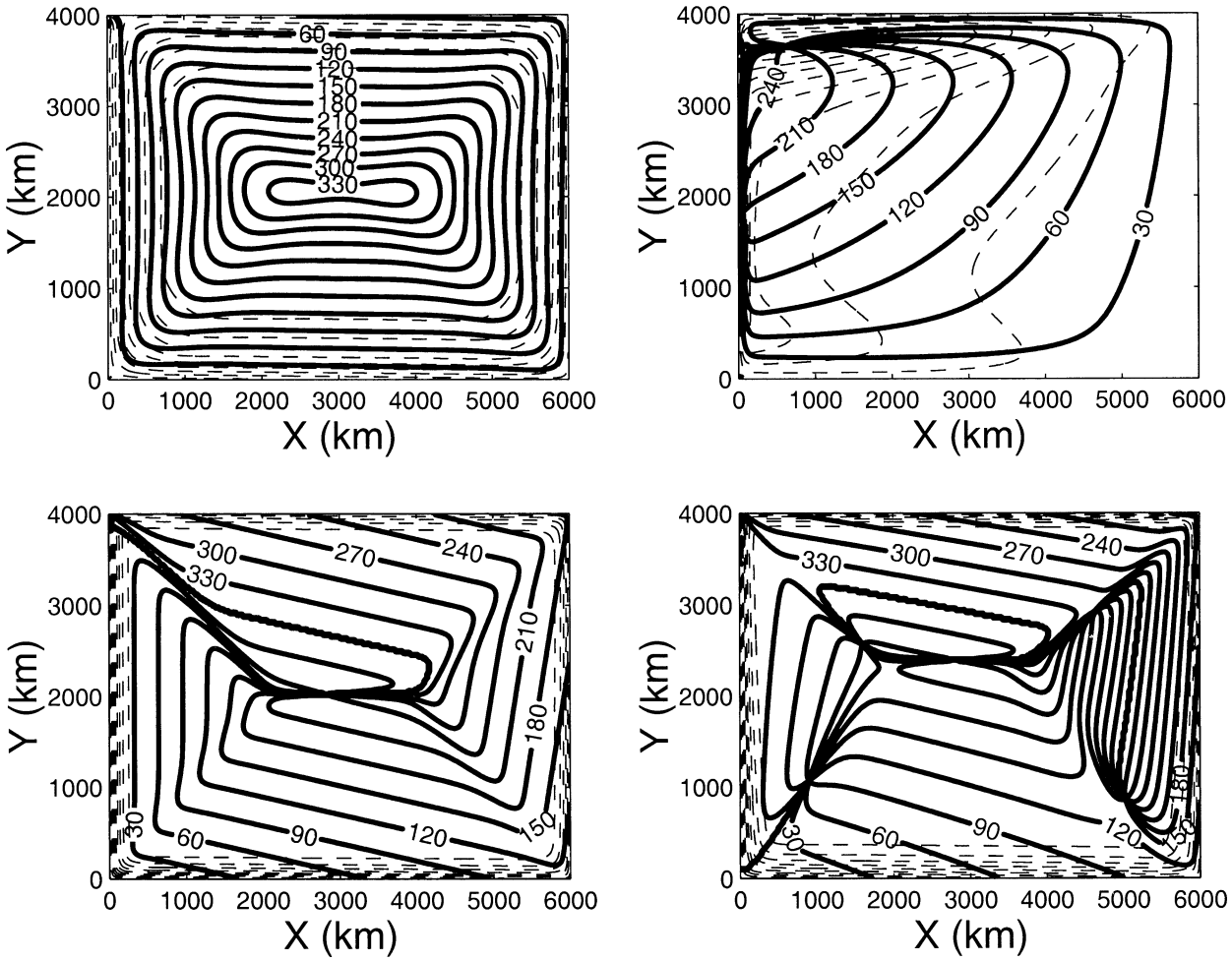

FIG. 15. Forced response in which the thickness h is prescribed to oscillate in time along the western boundary: (left panels) The response on an f plane and (right panels) the response on a β plane. (upper panels) The response for a forcing frequency of $\omega = 2\pi/756$ days^{-1}; (lower panels) The forced response for a forcing frequency of $\omega = 2\pi/25$ days^{-1}. The thick solid and dashed lines denote contours of phase and amplitude. The contour interval for the amplitude is 0.1. The amplitude is equal to unity along the boundary and decreases to zero toward the interior of the basin in all cases except the upper-right panel where the response decreases to zero at the amphidromic point near the northwest corner of the basin.

uniform boundary pressure fluctuation returns the energy to the eastern boundary, even when the speed of Kelvin waves is finite.

We find in the present study that it is the shape of the basin that determines the ability of the modes to be resonantly excited. If the basin shape is such that the basin crossing time for the long Rossby wave is a function of latitude, the modes' damping rate will remain finite and become independent of the friction parameter as the friction parameter is decreased. Nevertheless, we find that the resulting decay rate is sufficiently small for the modes to have real Q factors so that spectral peaks might be detectable. In fact, Cessi and Louazel (2001) have demonstrated that this is indeed the case through time-dependent simulations of the planetary geostrophic equations. Here we have focused on clarifying how the shape of the basin determines the modes decay rate by controlling the partition of energy that is either dissipated in the western boundary layer or transmitted back to the eastern boundary via a forced gravity wave response.

Finally, we caution on the use of rectangular ocean basins for theoretical studies of low-frequency variability using the quasigeostrophic equations. Rectangular basins are widely used for theoretical studies of the wind-driven ocean circulation because of the ease with which the boundary conditions can be applied in analytical and finite difference models. For quasigeostrophic dynamics, however, the rectangular basin is singular in the sense that it is an optimal resonator for long-wave basin modes. For the shallow-water equations, the optimal basin geometry has its width narrowing to the north such that the long-wave basin-crossing time becomes independent of latitude. For a basin geometry similar to the North Pacific with a wall along

the equator, we obtain Q factors of 0.6 and 1.2 for the two gravest modes. These estimates would of course decrease if the modes coupled strongly to other modes in the vertical because of topography for example. Nevertheless, if low-frequency long-wave modes are being excited by atmospheric forcing their Q factors appear to be sufficiently large for spectral peaks to be detectable in long records of the thermocline displacement.

Acknowledgments. Numerous conversations with Paola Cessi, as well as useful suggestions from the two anonymous reviewers, are gratefully acknowledged. The author wishes to acknowledge the use Jonathan Richard Shewchuk's ''Triangle'' program for two-dimensional quality mesh generation, available through Netlib. It was used for generating meshes for all the two-dimensional finite element computations.

REFERENCES

Cane, M. A., and E. S. Sarachik, 1977: Forced baroclinic ocean motions. II: The linear equatorial bounded case. *J. Mar. Res.*, **35,** 395–432.

——, and D. W. Moore, 1981: A note on low-frequency equatorial basin modes. *J. Phys. Oceanogr.*, **11,** 1578–1584.

Cessi, P., and S. Louazel, 2001: Decadal oceanic response to stochastic wind forcing. *J. Phys. Oceanogr.*, **31,** 3020–3029.

——, and F. Primeau, 2001: Dissipative selection of low-frequency modes in a reduced-gravity basin. *J. Phys. Oceanogr.*, **31,** 127–137.

Flierl, G. R., 1977: Simple applications of McWilliam's ''A note on a consistent quasi-geostrophic model in a multiply connected domain.'' *Dyn. Atmos. Oceans.*, **1,** 443–453.

LaCasce, J. H., 2000: Baroclinic Rossby waves in a square basin. *J. Phys. Oceanogr.*, **30,** 3161–3178.

Marion, J. B., 1970: *Classical Dynamics of Particles and Systems.* Academic Press, 573 pp.

Rao, D. B., 1966: Free gravitational oscillations in rotating rectangular basins. *J. Fluid Mech.*, **25,** 523–555.

Wunsch, C., 2000: On sharp spectral lines in the climate record and the millennial peak. *Paleoceanography*, **15,** 417–423.